RSC Advances

PAPER

View Article Online
View Journal | View Issue



Cite this: *RSC Adv.*, 2017, **7**, 45066

# Synthesis and characterization of free-standing activated carbon/reduced graphene oxide film electrodes for flexible supercapacitors

Lanshu Xu, Yue Li, Mengying Jia, Qiang Zhao, Xiaojuan Jin* and Chunli Yao*

Received 6th July 2017
Accepted 15th September 2017

DOI: 10.1039/c7ra07459j

rsc.li/rsc-advances

Free-standing, binder-free and flexible activated carbon/reduced graphene oxide (AC/rGO) composite films with various ratios were fabricated *via* a facile vacuum-filtration process. It was proved that two-dimensional rGO sheets were an ideal adhesive support for AC. The optimal ratio (AC : rGO = 2 : 1) was determined and the film electrodes displayed a high area specific capacitance of 486 mF $cm^{-2}$ with a mass of 2.35 mg $cm^{-2}$ (specific capacitance of 207 F $g^{-1}$) at 0.2 mA $cm^{-2}$. The assembled supercapacitor had the advantages of being flexible, lightweight, cheap and environmentally friendly, and can achieve a superior energy density of 16.2 μW h $cm^{-2}$ at a power density of 100 μW $cm^{-2}$ and 85% capacitance retention after 10 000 charging/discharging cycles. Moreover, 90% of the capacitance was retained after 1000 bending cycles and there was almost no performance change under different bending angles. These results well demonstrated a great potential for application of AC/rGO film electrodes in wearable and portable electronics.



## 1. Introduction

Flexible energy devices have drawn wide attention due to their potential application prospect in portable and wearable electronics.[1,2] Compared with traditional energy devices, a flexible power source can not only ensure good stability, high efficiency, safety and other basic requirements, but also store or convert energy upon bending or folding repeatedly without drastic decreasing of its performance.[3,4] Among them, flexible supercapacitors, with faster charging or discharging rate capability, longer life-cycles, and higher energy density, have attracted more and more research interest in the electrical energy storage field. Furthermore, a free-standing, ultrathin, miniaturized and binder-free electrode with large capacitance and low cost is an urgent requirement for flexible supercapacitors.[5]

Based on the charge storage mechanism, pseudocapacitive materials such as conductive polymers, as well as metal oxides and hydroxides, metal nitride and metal carbide can deliver higher capacitance *via* redox reaction.[6–8] Relatively speaking, carbon materials such as activated carbon (AC), carbon nanotubes, carbon fibers or graphene, are derived from natural resources and have been regarded as ideal substitutes of metal materials,[9,10] which present good rate capability and excellent cycling stability *via* reversible ion adsorption/desorption.[11–13] Especially for graphene with two-dimensional honeycomb structure, high surface area and high carrier mobility, possesses excellent mechanical flexibility and good electrical conductivity.[14] However, its compact lamellar structure and the easily caused agglomeration reduce the efficiency of specific surface area and affect the infiltration of electrolyte, which result in the graphite cannot suitable for supercapacitors. So far, various methods have been used for the graphene-based composites to solve this problem, such as hydrothermal method,[15,16] chemical vapour deposition (CVD),[5] electrophoretic deposition,[17] spin coating[18] and layer-by-layer self-assembling.[19] The transition metal oxides and hydroxides,[20–22] conducting polymers,[23–25] and biomass materials[26,27] were composited with graphene-based materials and widely developed in flexible electrode materials. However, carbon–carbon composites have rarely been reported.

ACs as the earliest and the most widely application of electrode materials, are hardly ever reported in flexible supercapacitor. AC materials are generally abundant, renewable, environmental friendliness and relatively low price,[28] which mainly come from the timber, nut hull, coconut shell, walnut shell, jujube shell, apricot shell, *etc.* Moreover, AC electrode has prominent properties such as easy process ability, higher pore content, larger specific surface area, and higher electrochemical stability.[29] However, the powder-like AC is difficult to handle as flexible electrode materials, binders (poly(vinylidene fluoride) (PVDF)) or (poly(tetrafluoroethylene) (PTFE)) are always needed in composites.[30–32] Therefore, it may be a good decision to choose ACs as intermediates, and graphene as an ideal binder and supporter for flexible supercapacitor electrode materials.

Herein, we reported a novel activated carbon/reduced graphene oxide (AC/rGO) film as the electrode material of flexible

*MOE Engineering Research Center of Forestry Biomass Materials and Bioenergy, Beijing Key Laboratory of Lignocellulosic Chemistry, Beijing Forestry University, Beijing 100083, China. E-mail: jxj0322@bjfu.edu.cn; chunliyao2006@163.com; Tel: +86-010-62337178*

supercapacitor, in which ACs, derived from waste fiberboard, were assembled with graphene obtained by chemically reduced graphene oxide. For the first time, free-standing, binder-free, flexible and lightweight AC/rGO film electrodes were obtained by vacuum filtration method. Three-dimensional porous AC/rGO film electrodes could achieve a significant synergistic effect. The morphology structures as well as electrochemical performances of different ratios of AC/rGO film electrodes were discussed and the optimum proportion was explored. As expected, the flexible supercapacitor possessed excellent mechanical property and remarkable electrochemical performances.

## 2. Experimental

### 2.1. Preparation of porous AC materials

Waste fiberboards as raw materials were supplied by Beijing Jiahekailai Furniture and Design Company, which contained 12 wt% urea–formaldehyde resin adhesive. Firstly, the raw materials were carbonized in a high-purity nitrogen atmosphere and heated to the temperature of 500 °C at the heating rate of 10 °C $min^{-1}$, then maintained for 60 min. After carbonization, the obtained materials were mixed with KOH at the mass ratio of 1 : 3 and further activated at the temperature of 750 °C for 60 min in oven. Finally, the activated ACs were washed and filtered using deionized water and 1 M HCl solution respectively until to neutral pH, and dried at 105 °C for 8 h, then stored for subsequent use.[17,32]

### 2.2. Synthesis of AC/rGO film electrodes

The graphene oxide (GO) was obtained by chemical treatment of natural graphite powders according to the modified Hummers' method.[33,34] Specifically, the obtained GO solution was carefully diluted into 2 mg $mL^{-1}$ using deionized water. The AC powder and acetylene black with a mass ratio of 9 : 1 were mixed and dispersed in *N*,*N*-dimethylformamide (DMF) to produce a homogeneous dispersion. The preparation procedure of AC/rGO composite films was depicted in Fig. 1. Based on the premise of ensuring the formation of flexible film, 5 mL of GO aqueous dispersion was mixed with 40, 20, 10 and 6.7 mL of AC (0.5 mg $mL^{-1}$) dispersion respectively, corresponding to add 5, 25, 35 and 38.3 mL of DMF in Erlenmeyer flask to ensure that the volume ratio of deionized water to DMF was 1 : 9, which was advantageous to improve the dispersion of GO.[35] Then the Erlenmeyer flasks were sealed with preservative film and under ultrasonic vibration for 2 h. Subsequently, a small quantity of hydrazine hydrate (80%) was added in the resulting homogeneous dispersion to chemically reduce GO. The weight ratio of hydrazine hydrate to GO was about 7 : 10.[36] After being vigorously shaken or stirred for 5 min, the Erlenmeyer flasks were put in a water bath (~95 °C) for 3 h. Finally, the mixture solution was vacuum-filtrated using an organic microporous membrane (50 mm in diameter, 0.45 μm in pore size). For comparison, the pure rGO solution was treated in the same procedure, and the obtained films were marked as AC : rGO = 2 : 1, AC : rGO = 1 : 1, AC : rGO = 1 : 2, AC : rGO = 1 : 3, rGO, respectively.

### 2.3. Assembly of flexible supercapacitors

First of all, two pieces of AC : rGO = 2 : 1 (1 cm × 3 cm) film electrodes and polypropylene membrane were immersed in the hot $H_2SO_4$/Polyvinyl alcohol (PVA) gel electrolyte (3 g $H_2SO_4$ and 3 g PVA were added into 30 mL deionized water) for 60 min, and subsequently picked out for air-drying to evaporate the residual water in the electrolyte and polypropylene membrane. After that, the film electrodes were connected with conductive copper wire (~0.2 mm in diameter) through conductive silver paste. A single piece of polypropylene membrane, sandwiched in between, was used as a separator to assembly the electrodes, then they were packaged together by PET film and pressed under a pressure of ~1 MPa for 10 min, which can make the electrodes adhered tightly and facilitate the electrolyte penetrating into them.

### 2.4. Characterizations

The substructure morphology and characteristics of the samples were examined by scanning electron microscope (SEM) (JEOL6500F) and transmission electron microscopy (TEM, JEM-1010), X-ray photoelectron spectroscopy (XPS) (AXIS Supra/Ultra), Raman spectra (Renishaw Raman RE01scope) and Brunauer–Emmett–Teller (BET) (Quantachrome Instruments). All samples were cut into circular sheets of 11 mm diameter to test

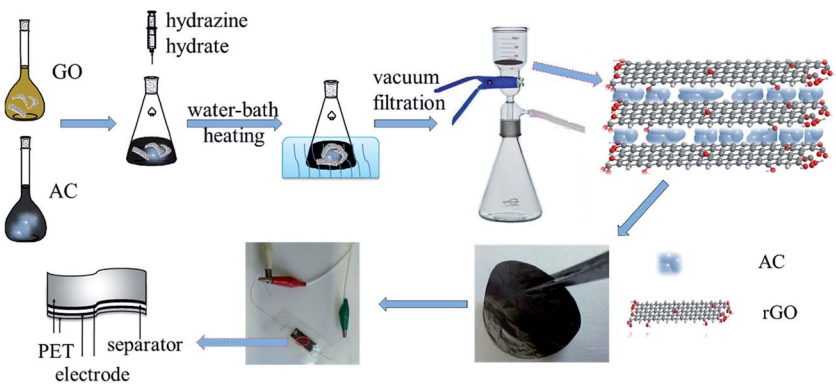


Fig. 1 Illustration of the preparation procedure of AC/rGO films.

the electrochemical performances. Moreover, the optimal one was processed into 1 cm × 3 cm slice to measure the mechanical flexibility. All electrochemical performances of the samples, including cyclic voltammetry (CV), galvanostatic charge/discharge (GCD) and impedance spectroscopy (EIS) curves were measured by a CHI 660D electrochemical workstation using a three-electrode system, in which platinum plate electrode and saturated calomel electrode were used as counter electrode and reference electrode respectively in an 1 M $H_2SO_4$ aqueous solution. The area specific capacitance ($C$, mF cm$^{-2}$) of single electrode or supercapacitor, the energy density ($E$, W h cm$^{-2}$), and power density ($P$, W cm$^{-2}$) was calculated by GCD curves using the following equations:[20,37]

$$C = \frac{i \times \Delta t}{S \times \Delta V} \quad (1)$$

$$E = \frac{1}{2} C \Delta V^2 \quad (2)$$

$$P = \frac{E}{\Delta t} \quad (3)$$

where $i$ (A) is the charge/discharge current, $\Delta t$ (h) is the discharging time, $S$ (cm$^{-2}$) is the surface area of one electrode, and $\Delta V$ ($V_f - V_i$) is the potential window.

## 3. Results and discussion

### 3.1. Characterization of the AC/rGO flexible electrodes

Fig. 2 displayed the substructure morphology and characteristics of the samples. The TEM image of pure GO sheets were showed in Fig. 2a, from that we can see the obtained GO was very well dispersed as a single-layer sheet, although the layered graphene tended to stack together to form agglomerate due to the chemical inertness. The SEM image in Fig. 2b reflected the AC particles have irregular shapes and a relatively smooth surface, indicating the structures of micropores and mesoporous cannot be detected by the ordinary SEM analysis. Fig. 2c–f showed the SEM images of AC : rGO = 1 : 3, 2 : 1 film electrodes at different magnifications, from which can be seen that film electrodes had a significant differences. In top-view SEM images (Fig. 2c and e), the ACs in AC/rGO composite films were coated with wavy and wrinkled rGO sheets layer by layer. The two-dimensional rGO sheets resembled adhesive to connect ACs together and provided a conductive bridge for ion transport. In addition, the surface became hillier with the increase of ACs proportion. Meanwhile, in the cross-section SEM images (Fig. 2d and f), we can observe the hierarchical structures of the composite films at the same magnification. Notably, the layer spacing was dramatically expanded by ACs (the thicknesses of composite films increased from 24 to 33 μm), which benefited to the infiltration and transmission of the electrolyte.

The XPS spectra of C 1s peaks for GO and rGO were shown in Fig. 3a and b. Four peaks were deconvoluted from the XPS spectra and distributed in the binding energies of 284.9, 286.7, 288.9 eV, which corresponded to the C=C, C–O, –C=O and –COO– bonds, respectively.[16,38,39] The results indicated the existence of oxygenated functional groups on the GO. Similar peaks were appeared in Fig. 3b, oxygenated carbon peaks markedly decreased compared with GO. The residual oxygen content is about 13.19% of the total element after chemical reduction of hydrazine hydrate. Although chemical reduction did not completely remove oxygen-containing functional groups, the flexibility and mechanical strength of AC/rGO films were well maintained.[19] Additionally, the whole XPS spectra of GO and rGO were shown in Fig. 3c. From that we can see the peak of the O element decreased significantly after chemical reduction. Compared with the XPS spectrum of GO, a small peak (N 1s) appeared in the rGO spectrum, which was mainly due to the introduction of N element in the process of hydrazine hydrate reduction. Moreover, the calculated values of N element increased from 0.64% to 2.81%, which was beneficial for capacitance improvement. Fig. 3d showed Raman spectra of the AC/rGO composite films. Typically, the two first-order bands D

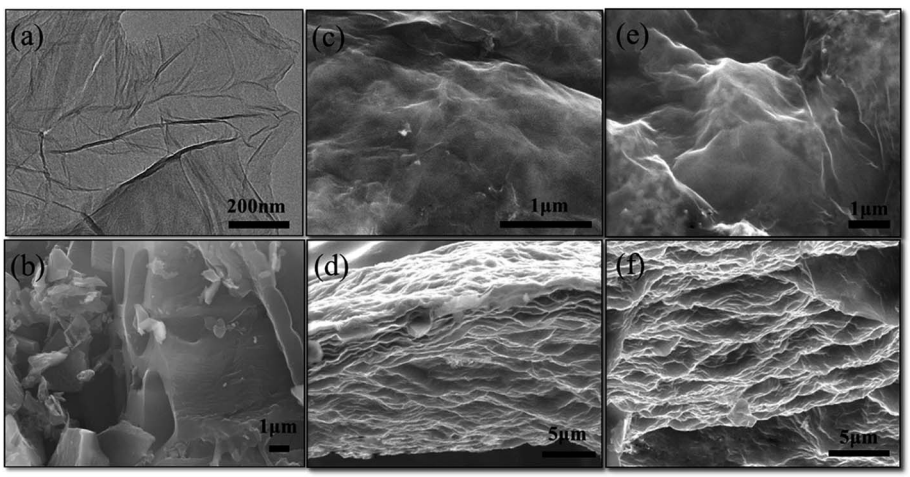


Fig. 2 (a) TEM image of pure GO sheets; (b) SEM image of pure ACs; (c, e) top-view, (d, f) cross-section SEM images of AC : rGO = 1 : 3, 2 : 1 film electrodes at different magnification.

 

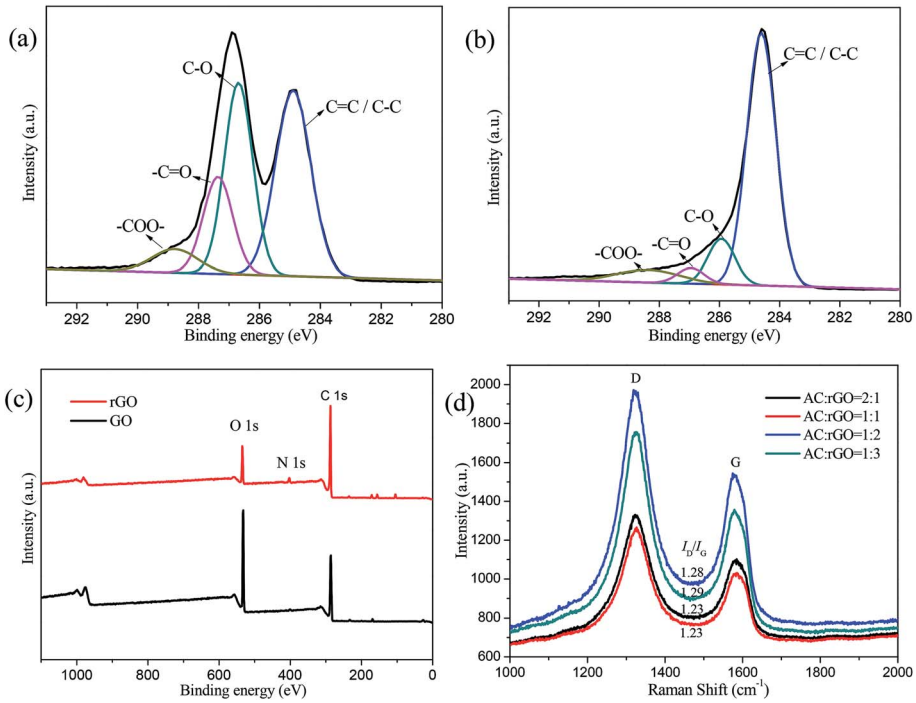


Fig. 3 High-resolution XPS spectra of C 1s peaks for (a) GO and (b) rGO; (c) the whole XPS spectra of GO and rGO; (d) Raman spectra of various ratios of the AC/rGO composites.

and a G were focused at the wave number of ~1335 cm$^{-1}$ and ~1590 cm$^{-1}$. In general, D peaks were stronger than G peaks, which indicated the composites had incomplete graphene structure and a large number of defects. The intensity ratio ($R = I_D/I_G$) of D peak induced by disordered structure and G peak caused by graphite crystal were used to characterize the disorder degree or defects of carbonaceous structures. As shown in Fig. 3d, with the proportion of the ACs increased, the $I_D/I_G$ ratio of different AC/rGO composites decreased slightly from 1.29 to 1.23, indicating that the degree of graphitization increased slightly.[40] It might be suggested that there were noncovalent interactions (might be hydrogen bonds, van der Waals force) between the AC/rGO composites, resulting in a good combination and excellent mechanical properties.[41,42]

The textural parameters of all samples were measured by typical $N_2$ adsorption/desorption isotherm at 77.35 K. From Fig. 4a, we can see that a typical sharp increase was appeared at a $P/P_0$ of 0.1, which was the characteristic of micropores of carbon-based material.[32] In particular, pure AC and the composites of AC : rGO = 2 : 1 and AC : rGO = 1 : 1 had a significant increase of the adsorbed volume.[43] The adsorption capacity improved significantly with the increase of the doping amount of ACs indicating that the surface area of AC/rGO composites increased dramatically with the increase feeding of porous ACs. The pore size distributions of all samples were shown in Fig. 4b. All samples were dominated by the micro size with radius around 0.5 to 0.8 nm, which contributed to the improvement of specific capacitance. Detailed information regarding the physical properties of all samples were listed in

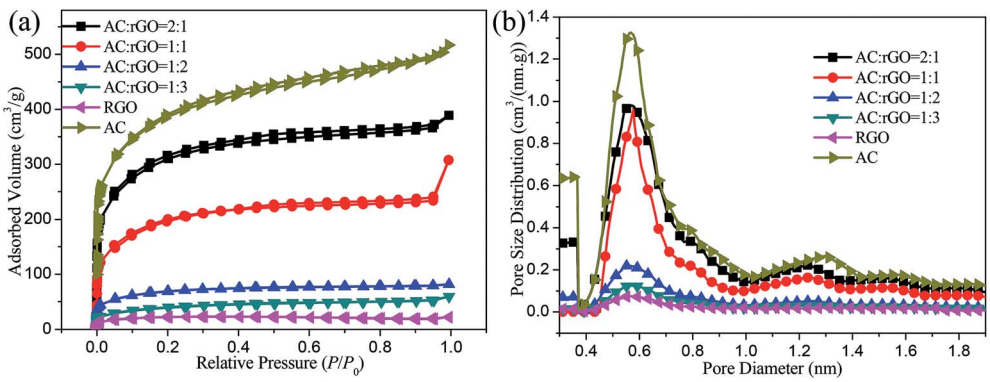


Fig. 4 (a) Nitrogen adsorption/desorption isotherms; (b) pore size distribution for all samples.

Table 1 Physical properties of all samples[a]

| Sample | $S_{BET}$ ($m^2$ $g^{-1}$) | $S_{mic}$ ($m^2$ $g^{-1}$) | $V_{tot}$ ($cm^3$ $g^{-1}$) | $V_{mic}$ ($cm^3$ $g^{-1}$) | $W_p$ (nm) |
|---|---|---|---|---|---|
| AC | 1204.0 | 914.7 | 0.7992 | 0.5053 | 0.568 |
| AC : rGO = 2 : 1 | 913.8 | 807.6 | 0.6021 | 0.4637 | 0.573 |
| AC : rGO = 1 : 1 | 552.0 | 495.1 | 0.4753 | 0.3062 | 0.578 |
| AC : rGO = 1 : 2 | 202.0 | 182.3 | 0.1264 | 0.1038 | 0.563 |
| AC : rGO = 1 : 3 | 104.5 | 79.91 | 0.0915 | 0.0559 | 0.578 |
| rGO | 89.81 | 78.99 | 0.0412 | 0.0338 | 0.579 |

[a] $S_{BET}$: the specific surface area; $S_{mic}$: the micropore surface area; $V_{tot}$: total pore volume; $V_{mic}$: micropore volume; $W_p$: average pore diameter.

Table 1. The pure AC sample had the largest specific surface area due to its porous structure. Moreover, the specific surface area ($S_{BET}$) of the AC/rGO composites doubled improved with the increase of AC proportion. Compared with others, the AC : rGO = 2 : 1 film electrodes exhibited the highest values for specific surface area and total pore volume at 931.8 $m^2$ $g^{-1}$ and 0.6021 $cm^3$ $g^{-1}$, respectively.

### 3.2. Electrochemical measurement

We characterized the electrochemical properties of the AC/rGO film electrodes in a three-electrode system with platinum plate electrode as counter electrode and saturated calomel electrode as reference electrode. The CV curves of all AC/rGO electrodes at the scan rate of 50 mV $s^{-1}$ were shown in Fig. 5a, all of CV curves were nearly rectangular in shape with a slight redox wave at around 0.6 V, indicating the presence of pseudocapacitance, which were probably due to the redox reaction of the residual oxygen containing functional groups on rGO sheets.[44] The nearly rectangular-shaped CV curves also indicated that the as-made electrodes had ideal charge performance.[32,45] Compared with others, the AC : rGO = 2 : 1 electrode showed much larger current and integral area. Further demonstration was tested and plotted in Fig. 5b, GCD curves of all electrodes showed triangular shape and the AC : rGO = 2 : 1 film electrodes had the longest time span, indicating that the doping amount of ACs had a dominant contribution to the electrochemical performances. Furthermore, the area specific capacitances were calculated from GCD measurements using eqn (1). As shown in Fig. 5c, it can be found that the area specific capacitances of

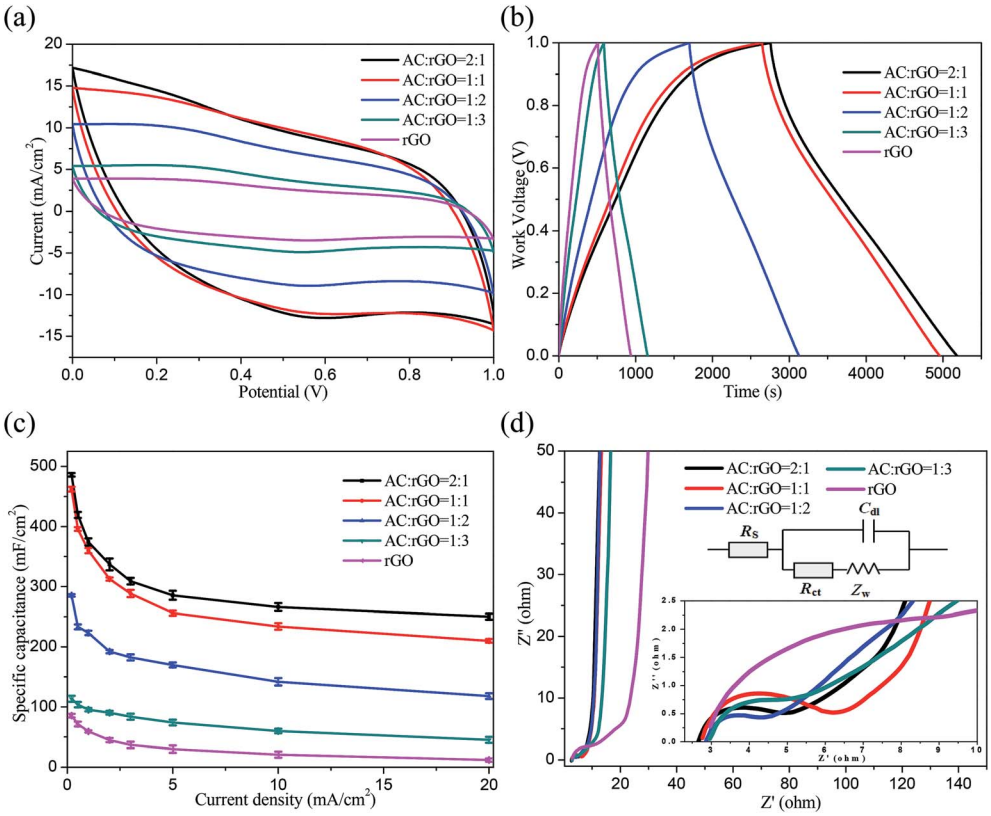


Fig. 5 (a) CV curves of all electrodes at the scan rate of 50 mV $s^{-1}$; (b) GCD curves of all electrodes at the current density of 0.2 mA $cm^{-2}$; (c) specific capacitance of all electrodes measured with different current densities; (d) Nyquist plot of all electrodes.

 

AC : rGO = 2 : 1 electrode were about 486, 420, 374, 337, 309 and 286 mF $cm^{-2}$ at current densities of 0.2, 0.5, 1, 2, 3 and 5 mA $cm^{-2}$, respectively. The highest area specific capacitance could reach 486 mF $cm^{-2}$ with a mass of 2.35 mg $cm^{-2}$ (specific capacitance of 207 F $g^{-1}$), which were much higher than others. The poor electrical conductivity of pure rGO film electrode could be ascribed to its compact lamellar structure in the process of vacuum extraction, which could prevent the transmission of electrolyte ions to some extent. We further used impedance spectroscopy to investigate film electrodes. Fig. 5d depicted the Nyquist plot starts from the $Z'$-axis and progresses almost vertically to the $Z''$-axis at the low frequency, indicating that the ideal capacitive characteristics of the electrodes. According to the semicircle intercepts of $Z'$, the charge transfer resistances ($R_{ct}$) of the AC : rGO = 2 : 1, 1 : 1, 1 : 2 and 1 : 3 film electrodes were 2.90, 3.82, 2.74 and 3.90 Ω, respectively. The corresponding total resistance ($R$) of the film electrodes were 5.56, 6.59, 5.61 and 6.86 Ω, respectively. In contrast, the pure rGO electrode had a large total resistance of 12.87 Ω, indicating that AC/rGO film electrodes with lower resistance had good conductivity. These results could be explained by synergistic effects of active materials: (i) the addition of ACs expanded the layer space and prevented the stacking of rGO sheets; (ii) the flexible connection of rGO sheets provided a conductive bridge for ACs; (iii) such a 3D AC/rGO composite films without any binders had a large specific surface area and good electrochemical performance, which could be used as flexible electrode directly.

In order to explore the electrochemical performances in practical application, a flexible supercapacitor with the optimal ratio of AC : rGO = 2 : 1 electrodes had been assembled and characterized. Fig. 6a showed CV curves of the flexible supercapacitor measured from 0 to 1.0 V at various scan rates. All of CV curves afforded deformed rectangular-like shapes even at high scan rates, which elucidated the ideal capacitive and fast charge/discharge behavior of the flexible supercapacitor. Meanwhile, GCD curves at different current densities were recorded to further evaluate the performance. Fig. 6b showed that the charging/discharging curves were nearly symmetric triangular shape with their corresponding discharging counterparts, further demonstrating an ideal capacitive behavior of the device. The area specific capacitances of flexible supercapacitor were calculated using eqn (1) and plotted in Fig. 6c. From that we can see the highest area specific capacitance was 116.8 mF $cm^{-2}$ at current density of 0.2 mA $cm^{-2}$. Upon increasing the current density up to 5 mA $cm^{-2}$, the specific capacitance retained about 52.6% of its original value. Additionally, approximately 85% capacitance was retained after 10 000 charging/discharging cycles at the current density of 5 mA $cm^{-2}$, indicating an excellent stability and efficacy of the rapid electron transfer during charge/discharge processes. A comparison of the energy and power density of flexible supercapacitor with various reported rGO composites was given in Fig. 6d. According to the eqn (2) and (3), the calculated energy density was 16.2 μW h $cm^{-2}$ at a power density of 100 μW $cm^{-2}$ at current density of 0.2 mA $cm^{-2}$. Evidently, the performance of

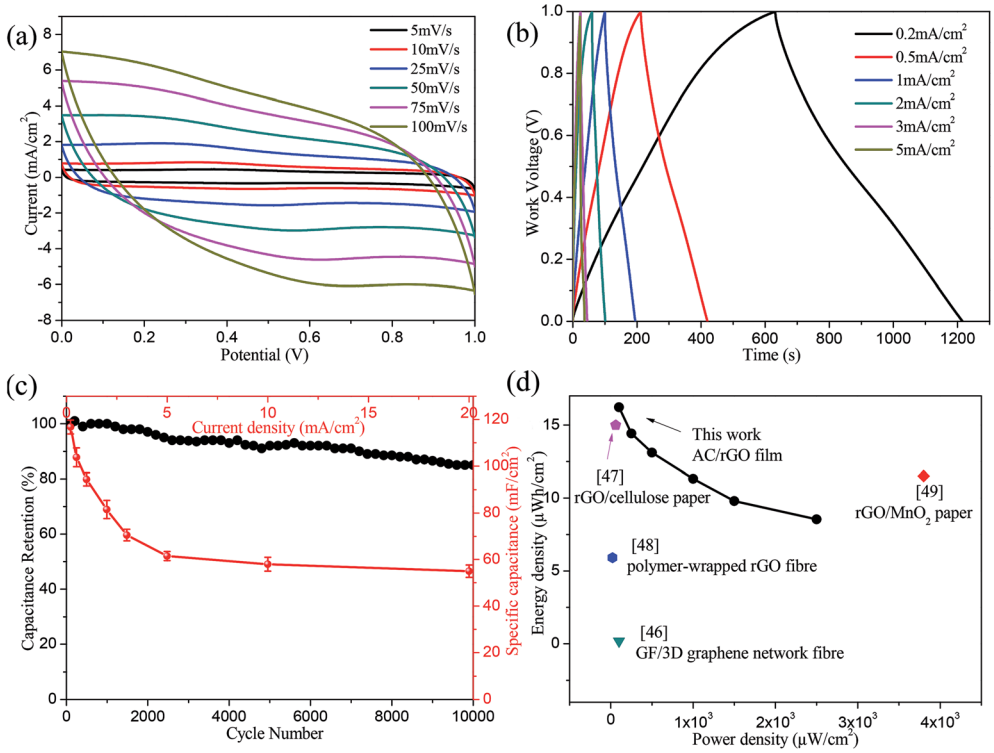


Fig. 6 (a) CV curves of flexible supercapacitor at different scan rates; (b) GCD curves and (c) specific capacitance of flexible supercapacitor at different current densities and cycling stability over 10 000 cycles at 5 mA $cm^{-2}$; (d) energy density as a function of power density.

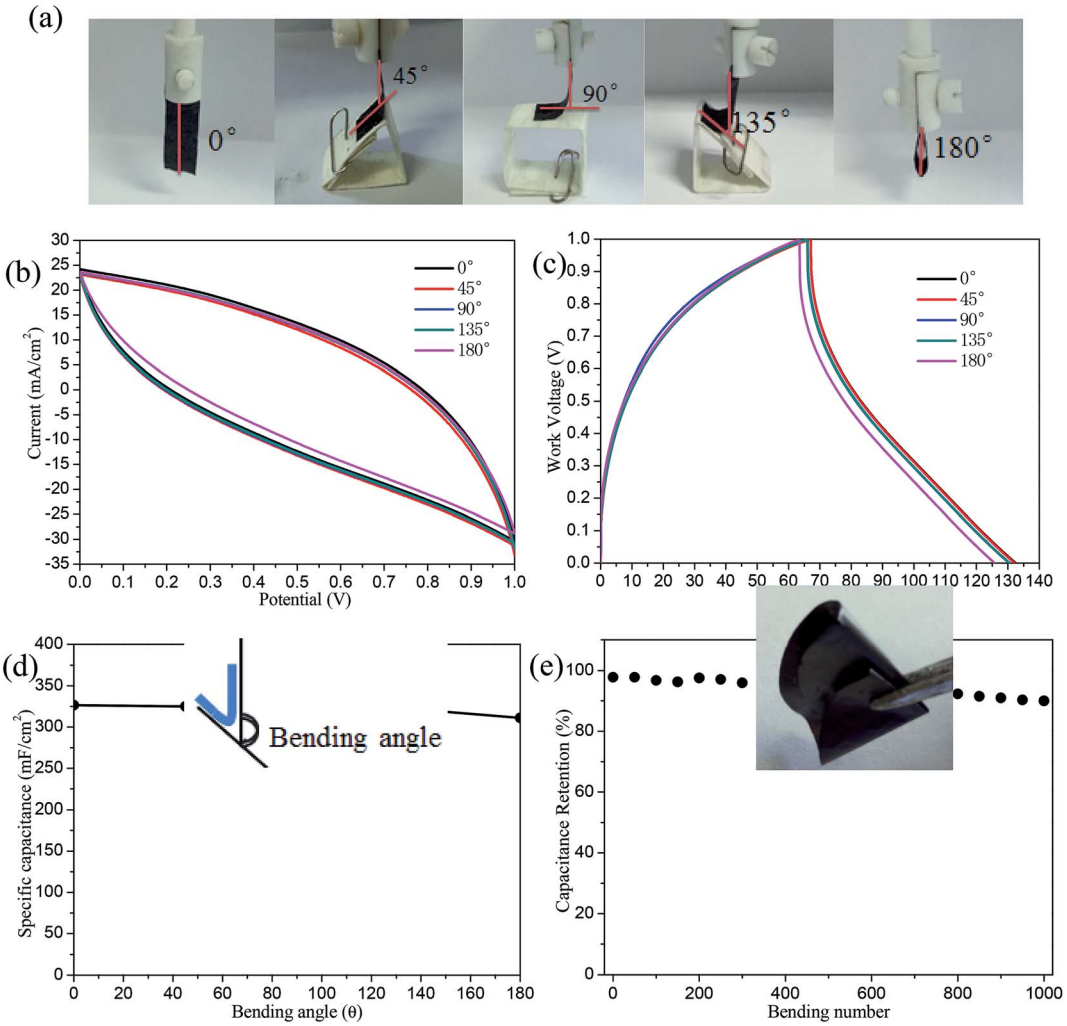


Fig. 7 (a) Photographs of the films bended to different angles; (b) CV and (c) GCD curves of the electrodes at different bending angle of 0°, 45°, 90°, 135°, and 180°; (d) specific capacitance at different bending angles; (e) efficiency of the films after different bending cycles at the current density of 5 mA $cm^{-2}$.

AC/rGO flexible device was superior to others, such as GF/3D graphene network fibre (100 μW $cm^{-2}$, 0.17 μW h $cm^{-2}$),[46] rGO/cellulose paper (60 μW $cm^{-2}$, 15 μW h $cm^{-2}$),[47] polymer-wrapped rGO fibre (20 μW $cm^{-2}$, 5.91 μW h $cm^{-2}$),[48] rGO/$MnO_2$ paper (3800 μW $cm^{-2}$, 11.5 μW h $cm^{-2}$).[49]

### 3.3. Electrochemical performance of bending film

The mechanical flexibility of the AC/rGO electrodes was intensively studied at different bending angles of 0°, 45°, 90°, 135°, and 180° (seen in Fig. 7a, the corresponding measurement images). As shown in Fig. 7b and c, CV and GCD curves were nearly overlapped at different bending angles, illustrating the flexible electrode had negligible influence on folding or bending angles. The corresponding specific capacitances were calculated by GCD curves (seen in Fig. 7d), there was only about 4.7% fading for the capacitance when bended to 180°, highlighting the excellent flexibility of AC/rGO electrodes. Fatigue test in Fig. 7e (photograph of the film can be folded arbitrarily) revealed that the specific capacitance of the flexible electrode maintained at 90% of the original value after 1000 cycles at a high current density of 5 mA $cm^{-2}$. Such a high capacitive retention was ascribed to favorable synergistic effect, electrochemical robustness and mechanical strength of the 3D layered structure of AC/rGO.

## 4. Conclusions

In summary, a facile method was used to successfully construct free-standing, binder-free, flexible and lightweight AC/rGO film electrodes with different ratios (AC : rGO = 2 : 1, AC : rGO = 1 : 1, AC : rGO = 1 : 2, AC : rGO = 1 : 3). With the increase of the doping amount of ACs, the area specific capacitance increased significantly. Based on the premise of ensuring the formation of flexible film, the optimal ratio (AC : rGO = 2 : 1) were determined and the film electrode could deliver a superior area specific capacitance of 486 mF $cm^{-2}$ with a mass of 2.35 mg $cm^{-2}$ (specific capacitance of 207 F $g^{-1}$) at 0.2 mA $cm^{-2}$. The assembled double layer flexible AC/rGO supercapacitor reached

 

high energy density of 16.2 μW h $cm^{-2}$ at a power density of 100 μW $cm^{-2}$ at 0.2 mA $cm^{-2}$, and its capacitance retention up to 85% after 10 000 charging/discharging cycles. Moreover, 90% of the capacitance was retained after 1000 bending cycles at 5 mA $cm^{-2}$ and almost no performance changed under different bending angles. Overall, these results well demonstrated that our flexible AC/rGO electrode is a promising candidate for assembling environment friendly, low price, ultrathin and flexible supercapacitors in wearable and portable electronic applications.

## Conflicts of interest

There are no conflicts to declare.

## Acknowledgements

This work greatly thanked to the support of the National Natural Science Foundation of China (31470605).

## References

1 X. Wang and G. Shi, *Energy Environ. Sci.*, 2015, **8**, 790–823.
2 H. Gwon, J. Hong, H. Kim, D. H. Seo, S. Jeon and K. Kang, *Energy Environ. Sci.*, 2014, **7**, 538–551.
3 H. Gwon, H. S. Kim, K. U. Lee, D. H. Seo, C. P. Yun, Y. S. Lee, B. T. Ahn and K. Kang, *Energy Environ. Sci.*, 2011, **4**, 1277–1283.
4 L. Zhang, P. Zhu, F. Zhou, W. Zeng, H. Su, G. Li, J. Gao, R. Sun and C.-p. Wong, *ACS Nano*, 2015, **10**, 1273–1282.
5 Y. He, W. Chen, X. Li, Z. Zhang, J. Fu, C. Zhao and E. Xie, *ACS Nano*, 2012, **7**, 174–182.
6 B. Gao, X. Li, X. Guo, X. Zhang, X. Peng, L. Wang, J. Fu, P. K. Chu and K. Huo, *Adv. Mater. Interfaces*, 2015, **2**, 1500211.
7 K. Wang, H. Wu, Y. Meng and Z. Wei, *Small*, 2014, **10**, 14–31.
8 V. Augustyn, P. Simon and B. Dunn, *Energy Environ. Sci.*, 2014, **7**, 1597–1614.
9 X. Lu, M. Yu, G. Wang, Y. Tong and Y. Li, *Energy Environ. Sci.*, 2014, **7**, 2160–2181.
10 K. Wu, J. Fu, X. Zhang, X. Peng, B. Gao and P. K. Chu, *Mater. Lett.*, 2016, **185**, 193–196.
11 X. Hu, W. Xiong, W. Wang, S. Qin, H. Cheng, Y. Zeng, B. Wang and Z. Zhu, *ACS Sustainable Chem. Eng.*, 2016, **4**, 1201–1211.
12 Y. Sun, R. B. Sills, X. Hu, Z. W. Seh, X. Xiao, H. Xu, W. Luo, H. Jin, Y. Xin and T. Li, *Nano Lett.*, 2015, **15**, 3899–3906.
13 M. Sevilla, L. Yu, L. Zhao, C. O. Ania and M.-M. Titiricic, *ACS Sustainable Chem. Eng.*, 2014, **2**, 1049–1055.
14 H. Tian, Y. Yang, D. Xie, T. L. Ren, Y. Shu, C. J. Zhou, H. Sun, X. Liu and C. H. Zhang, *Nanoscale*, 2013, **5**, 890–894.
15 J. Yu, J. Wu, H. Wang, A. Zhou, C. Huang, H. Bai and L. Li, *ACS Appl. Mater. Interfaces*, 2016, **8**, 4724–4729.
16 X. Wu, Q. Wang, W. Zhang, Y. Wang and W. Chen, *Electrochim. Acta*, 2016, **211**, 1066–1075.
17 H. R. Yu, S. Cho, M. J. Jung and Y. S. Lee, *Microporous Mesoporous Mater.*, 2013, **172**, 131–135.
18 A. Ramadoss, B. Saravanakumar and J. K. Sang, *Nano Energy*, 2015, **15**, 587–597.
19 Y. Yu, Y. Zhai, H. Liu and L. Li, *Mater. Lett.*, 2016, **176**, 33–37.
20 M. S. Javed, S. Dai, M. Wang, D. Guo, L. Chen, X. Wang, C. Hu and Y. Xi, *J. Power Sources*, 2015, **285**, 63–69.
21 J. Zhang, X. Zhao, Z. Huang, T. Xu and Q. Zhang, *Carbon*, 2016, **107**, 844–851.
22 Z. Pan, Y. Qiu, J. Yang, F. Ye, Y. Xu, X. Zhang, M. Liu and Y. Zhang, *Nano Energy*, 2016, **26**, 610–619.
23 M. Gholami, P. M. Nia, L. Narimani, M. Sokhakian and Y. Alias, *Appl. Surf. Sci.*, 2016, **378**, 259–269.
24 X. L. Song, J. X. Guo, M. X. Guo, D. Z. Jia, Z. P. Sun and L. X. Wang, *Electrochim. Acta*, 2016, **206**, 337–345.
25 Q. Wu, Y. Xu, Z. Yao, A. Liu and G. Shi, *ACS Nano*, 2010, **4**, 1963–1970.
26 K. Gao, Z. Shao, J. Li, X. Wang, X. Peng, W. Wang and F. Wang, *J. Mater. Chem.*, 2013, **1**, 63–67.
27 N. D. Luong, N. Pahimanolis, U. Hippi, J. T. Korhonen, J. Ruokolainen, L. S. Johansson, J. D. Nam and J. Seppälä, *J. Mater. Chem.*, 2011, **21**, 13991–13998.
28 Y. Lv, L. Gan, M. Liu, W. Xiong, Z. Xu, D. Zhu and D. S. Wright, *J. Power Sources*, 2012, **209**, 152–157.
29 T. X. Shang, Y. M. Zhu and X. J. Jin, *Sci. Adv. Mater.*, 2016, **8**, 1101–1107.
30 Y. Chen, X. Zhang, H. Zhang, X. Sun, D. Zhang and Y. Ma, *RSC Adv.*, 2012, **2**, 7747–7753.
31 C. Zheng, X. Zhou, H. Cao, G. Wang and Z. Liu, *J. Power Sources*, 2014, **258**, 290–296.
32 T. X. Shang, R. Q. Ren, Y. M. Zhu and X. J. Jin, *Electrochim. Acta*, 2015, **163**, 32–40.
33 W. S. Hummers Jr and R. E. Offeman, *J. Am. Chem. Soc.*, 1958, **80**, 1339.
34 N. I. Kovtyukhova, P. J. Ollivier, B. R. Martin, T. E. Mallouk, S. A. Chizhik, E. V. Buzaneva and A. D. Gorchinskiy, *Chem. Mater.*, 1999, **11**, 771–778.
35 S. Park, J. An, I. Jung, R. D. Piner, S. J. An, X. Li, A. Velamakanni and R. S. Ruoff, *Nano Lett.*, 2009, **9**, 1593–1597.
36 D. Li, M. B. Müller, S. Gilje, R. B. Kaner and G. G. Wallace, *Nat. Nanotechnol.*, 2008, **3**, 101–105.
37 Y. Liu, X. Miao, J. Fang, X. Zhang, S. Chen, W. Li, W. Feng, Y. Chen, W. Wang and Y. Zhang, *ACS Appl. Mater. Interfaces*, 2016, **8**, 5251–5260.
38 P. Yu, Y. Li, X. Zhao, L. Wu and Q. Zhang, *Langmuir*, 2014, **30**, 5306–5313.
39 B. Guo, Q. Liu, E. Chen, H. Zhu, L. Fang and J. R. Gong, *Nano Lett.*, 2010, **10**, 4975–4980.
40 J.-S. Roh, *Carbon Letters*, 2008, **9**, 127–130.
41 Y. Liu, L. Gao and J. Sun, *J. Phys. Chem. C*, 2007, **111**, 1223–1229.
42 F. Li, X. Wang, T. Yuan and R. Sun, *J. Mater. Chem. A*, 2016, **4**, 11888–11896.
43 D. Prahas, Y. Kartika, N. Indraswati and S. Ismadji, *Chem. Eng. J.*, 2008, **140**, 32–42.
44 J. Zhu, M. Chen, H. Qu, X. Zhang, H. Wei, Z. Luo, H. A. Colorado, S. Wei and Z. Guo, *Polymer*, 2012, **53**, 5953–5964.

45 P. L. Taberna, P. Simon and J. F. Fauvarque, *J. Electrochem. Soc.*, 2003, **150**, A292–A300.
46 Y. Meng, Y. Zhao, C. Hu, H. Cheng, Y. Hu, Z. Zhang, G. Shi and L. Qu, *Adv. Mater.*, 2013, **25**, 2326–2331.
47 W. Zhe, S. Yang, D. W. Wang, L. Feng, J. Du and H. M. Cheng, *Adv. Energy Mater.*, 2011, **1**, 917–922.
48 L. Kou, T. Huang, B. Zheng, Y. Han, X. Zhao, K. Gopalsamy, H. Sun and C. Gao, *Nat. Commun.*, 2014, **5**, 3754.
49 A. Sumboja, C. Y. Foo, X. Wang and P. S. Lee, *Adv. Mater.*, 2013, **25**, 2809–2815.